



Retracking of SARAL/AltiKa Radar Altimetry Waveforms for Optimal Gravity Field Recovery

Shengjun Zhang & David T. Sandwell

To cite this article: Shengjun Zhang & David T. Sandwell (2016): Retracking of SARAL/AltiKa Radar Altimetry Waveforms for Optimal Gravity Field Recovery, Marine Geodesy, DOI: [10.1080/01490419.2016.1265032](https://doi.org/10.1080/01490419.2016.1265032)

To link to this article: <http://dx.doi.org/10.1080/01490419.2016.1265032>



Accepted author version posted online: 30 Nov 2016.
Published online: 30 Nov 2016.



Submit your article to this journal [↗](#)



Article views: 38



View related articles [↗](#)



View Crossmark data [↗](#)

Retracking of SARAL/AltiKa Radar Altimetry Waveforms for Optimal Gravity Field Recovery

Shengjun Zhang^a and David T. Sandwell^b

^aSchool of Geodesy and Geomatics, Wuhan University, Wuhan, China; ^bScripps Institution of Oceanography, University of California at San Diego, La Jolla, California, USA

ABSTRACT

The accuracy of the marine gravity field derived from satellite altimetry depends on dense track spacing as well as high range precision. Here, we investigate the range precision that can be achieved using a new shorter wavelength Ka-band altimeter AltiKa aboard the SARAL spacecraft. We agree with a previous study that found that the range precision given in the SARAL/AltiKa Geophysical Data Records is more precise than that of Ku-band altimeter by a factor of two. Moreover, we show that two-pass retracking can further improve the range precision by a factor of 1.7 with respect to the 40 Hz-retracked data (item of range_40 hz) provided in the Geophysical Data Records. The important conclusion is that a dedicated Ka-band altimeter-mapping mission could substantially improve the global accuracy of the marine gravity field with complete coverage and a track spacing of <6 km achievable in ~1.3 years. This would reveal thousands of uncharted seamounts on the ocean floor as well as important tectonic features such as microplates and abyssal hill fabric.

ARTICLE HISTORY

Received 17 April 2016
Accepted 22 November 2016

KEYWORDS

Gravity field; noise level; SARAL/AltiKa; waveform retracking

Introduction

Over the past 40 years, satellite altimetry has evolved as an accurate and effective method for recovering the global marine gravity field (Rapp 1979; Haxby et al. 1983; Sandwell and Smith 1997; Andersen and Knudsen 1998; Hwang et al. 1998; Sandwell et al. 2014). Gravity field accuracy depends primarily on two factors: spatial track density and altimeter range precision. Here, we investigate the improved range precision provided by the AltiKa altimeter aboard the SARAL spacecraft (Vincent et al. 2006; Verron et al. 2015). The main technical innovation in the AltiKa altimeter is that it operates at a shorter wavelength Ka-band (8.4 mm wavelength) than all previous altimeters, which operate at Ku-band (22 mm) or longer wavelength. The shorter wavelength enables three key improvements (Raney and Phalippou 2011): (1) A higher chirp bandwidth at Ka-band corresponds to a shorter radar pulse and a smaller gate spacing of 0.31 m versus 0.47 m. Theoretically, this should result in a factor of ~1.52 improvement in range precision over a flat ocean (Chelton et al. 2001), but

CONTACT David T. Sandwell ✉ dsandwell@ucsd.edu ✉ Scripps Institution of Oceanography, University of California at San Diego, La Jolla, CA 92037, USA.

Color versions of one or more of the figures in the article can be found online at www.tandfonline.com/umgd.

© 2017 Taylor & Francis Group, LLC

this improvement will be diminished when the ocean surface is roughened by waves having significant wave height (SWH) typically ≥ 2 m (Smith 2015). (2) While AltiKa's antenna diameter (1 m) is about the same as those of previous missions, the shorter carrier wavelength results in a narrower beam width (8.9 km versus 21 km subtended on Earth's surface). (3) The shorter wavelength allows faster decorrelation of echoes, allowing the pulse repetition frequency (PRF) to be set higher. The combined effects of these improvements are expected to result in a factor of ~ 2 improvement in range precision (Raney and Phalippou 2011). This is important because it demonstrates that a complete mapping of the sea surface topography using this new technology could significantly improve the accuracy of the global marine gravity field (Smith 2015). The main disadvantage of Ka-band altimetry is that the shorter wavelength pulse is more susceptible to attenuation by water droplets than Ku-band pulse (Raney and Phalippou 2011). As a result, special attention should be paid to the rain-contaminated Ka-band altimeter waveforms (Tournadre et al. 2009).

A recent study by Smith (2015) has demonstrated a factor of 2 improvement in the range precision of AltiKa with respect to Envisat RA2. The noise spectra show white noise floors at root mean square (RMS) levels around 8 mm per root-Hz for AltiKa and 19 mm per root-Hz for RA2. However, Smith (2015) argues that there should be no benefit from the shorter pulse length of AltiKa because the leading edge of the pulse will be blurred after reflection from a rough ocean surface having a typical SWH of 2 m. Therefore, he notes that the observed noise reduction is greater than that one would expect from the ratio of PRF (i.e., about square root of 2). He attributes the additional range precision to the faster roll-off in the power of the trailing edge of AltiKa with respect to RA2. Moreover, an analysis of individual profiles of AltiKa, in comparison with RA2, shows improved resolution of short wavelength geoid anomalies such as those associated with small seamounts. While this analysis seems to confirm the expected noise reduction of Ka-band altimetry by a factor of 2 with respect to Ku-band altimetry predicted by Raney and Phalippou (2011), the two studies differ in the explanation for the full factor of two improvement. The Raney and Phalippou (2011) study invokes the shorter pulse length to explain the additional improvement, while Smith (2015) suggests the precision results from the more complex waveform shape and the faster tail roll-off. A third possibility suggested by one of the reviewers of this paper is that the additional range precision is due to the improved signal-to-noise ratio of the AltiKa altimeter with respect to previous altimeters. Here, we do not address or resolve the issue of why there is a full factor of two improvement. Instead, we are focused on the issue of how much the range precision can be further improved by application of a two-pass retracker that has been successful for Ku-band altimeters (Sandwell and Smith 2005; Garcia et al. 2014).

Waveform retracking is an effective and mature technique to solve limitations of data contamination by distribution of land or islands. There are many kinds of retracking algorithms based either on empirical statistics or model fitting (Martin et al. 1983; Wingham 1986; Laxon et al. 1994; Sarraillh et al. 1997; Hwang et al. 2006). Retracking of the raw altimeter waveforms can be customized for a variety of applications. Threshold-type retracker are used to improve the accuracy of data contaminated either by sea ice or land reflective surface (Davis 1995; Hwang et al. 2006). The advantage of these retracker is that they provide a robust estimate of range for complex waveform shapes. However, the precision of these methods is limited to the size of the gates (0.31 m for AltiKa). Specialized sub-waveform retracker provide optimal results in coastal regions (Idris and Deng 2012; Passaro et al.

2014). Over the open ocean, the shape of the waveform is well matched by the Brown (1977) model where the full shape of the waveform can be used to estimate five parameters—arrival time, rise time, amplitude, square of the antenna mispointing angle, and thermal noise. The first three parameters recovered from the Brown model are of interest for applications in physical oceanography as the arrival time provides an estimate of sea surface height, the rise time provides an estimate of SWH, and the power in the returned waveform provides an estimate of the surface radar cross section, which may be related to wind speed over the ocean surface (Chelton et al. 2001). A four-parameter retracking method (where thermal noise is treated as constant parameter in the weight function rather than a free parameter) was used to construct the geophysical data records (GDR) for AltiKa and Envisat RA2 used by Smith (2015) in his analysis of the noise characteristics of these two instruments. Previous studies (Maus et al. 1998; Sandwell and Smith 2005; Andersen and Knudsen 2010) have shown that errors in retracked estimates of arrival time and rise time are inherently correlated because of the noise characteristics of the returned waveform. For recovery of the marine gravity field, only the arrival time parameter is needed. One approach to improve the precision of the arrival time is to fix the rise time parameter to a value based on an average of the surrounding waveforms (Sandwell and Smith 2005). This can be accomplished with a two-pass retracking method where the waveforms are first retracked with the full three-parameter Brown model (arrival time, rise time, and amplitude). The rise time parameter is then smoothed along track, before retracking the waveforms a second time using a two-parameter Brown model (arrival time and amplitude) with the rise time being fixed to the along-track smoothed value (Sandwell and Smith 2005). Garcia et al. (2014) showed that this two-pass approach improves the range precision by a factor of ~ 1.5 for most conventional Ku-band altimeters considered in their study (Geosat/GM, ERS-1, Envisat, Jason-1, and CryoSat-2 LRM), but it does not result in an improvement in the precision of the arrival time for the more complex SAR waveform from CryoSat-2.

In this study, we firstly investigate whether two-pass retracking of the waveforms from the AltiKa altimeter also results in a factor of ~ 1.5 improvement in range precision. If the two-pass retracking procedure does not bring expected improvement for AltiKa, as in the case of CryoSat-2 SAR waveforms, then the Ka-band altimeter offers only a factor of 1.5 improvement in range precision with respect to Ku-band altimeters that do benefit from two-pass retracking. However, if the AltiKa range precision also benefits from the two-pass retracking method, then there could be a dramatic improvement in the global marine gravity field using this new technology on a geodetic mapping orbit. A second objective of our study is to compare the range precision of the AltiKa data to the Ku-band data from Envisat since it has the same ground track as SARAL and was also used in the Smith (2015) study.

Theory and data analysis

Average returned waveform model

The conventional pulse-limited radar altimeter transmits a series of pulses (that is, frequency-modulated chirps) toward the sea surface and records the power of the returned signals, which have interacted with the rough sea surface. The returned signal power is proportional to the illuminated area scaled by the off-nadir roll-off of the antenna gain pattern (Brown 1977; Chelton et al. 2001; Amarouche et al. 2004). For recovery of the gravity field, we are only interested in the slope of the sea surface height so, for example, the

constant offset with long-wave characteristics can be ignored. We also consider the case where the antenna bore sight is pointed to nadir. Under these simplifying assumptions, the power in the returned waveform can be modeled as (Rodriguez 1988).

$$M(t) = \frac{A}{2} \left[1 + \operatorname{erf} \left(\frac{t - t_o}{\sqrt{2}\sigma} \right) \right] \exp \left[-\alpha(t - t_o) \right] \quad (1)$$

where A is the amplitude, t_o is the arrival time, t is time for each sample gate, σ is the effective pulse length, and α is the trailing edge decay factor. The effective pulse length σ consists of two factors $\sigma^2 = \sigma_h^2 + \sigma_p^2$. The σ_h is the broadening of the pulse due to the interaction of ocean waves $\sigma_h = SWH/2c$, where SWH is the significant wave height and c is the speed of light. The $\sigma_p = 0.513\tau_p$ is the standard deviation of the length of the outgoing pulse where $\tau_p = 1/B$ and B is the chirp bandwidth (320 MHz for Ku and 480 MHz for SARAL/AltiKa) (Amarouche et al. 2004).

The model has three unknown parameters $[A, \tau_o, \sigma_h]$ that will be estimated using a weighted iterative least-squares approach, which is similar to the unweighted maximum likelihood estimator (Amarouche et al. 2004; Thibaut et al. 2010). In our analysis, we solve for a single value of α based on an analysis of randomly selected AltiKa profiles from cycle23. The chi-square measure of the misfit between the returned power samples P_i and the model estimate for the corresponding time t_i is

$$\chi^2 = \sum_{i=1}^N \left[\frac{P_i - M(t_i - t_o, \sigma_h, A, \alpha)}{W_i} \right]^2 \quad (2)$$

where N is the number of gates (i.e., time samples) in the waveform, and W_i is the uncertainty assigned to each sample and is given by

$$W_i = \frac{(P_i + P_o)}{\sqrt{K}} \quad (3)$$

where K is the number of statistically independent return echoes that were averaged to produce the waveform data records and P_o is the power offset value reflecting the thermal noise of the instrument. Actually, the estimated results using weighted least-squares approach are largely insensitive to the exact numerical values for K and P_o (Sandwell and Smith 2005).

Overall, there are six unknown parameters, but for our analysis, we will divide them into two groups: parameters $([A, t_o, \sigma_h])$ to be solved for each waveform and auxiliary parameters $([K, P_o, \alpha])$ to be pre-determined. We will assume that the two parameters, K and P_o , describing the uncertainty in the power in each gate, remain constant throughout the lifetime of the mission following the previous study by Garcia et al. (2014). Additionally, the trailing edge decay factor α depends on the antenna beam width, the altitude of the orbit, and the square of the off-nadir pointing angle. Height variations around the orbit have a negligible effect on α , and the only important source of variation in α is caused by variations in the bore sight of the antenna away from nadir. Fortunately, the mispointing errors are much less than the beamwidth of the antenna pattern (Pierre 2015; Steunou 2015), so we will adopt a constant value for this parameter based on an initial least-squares analysis of

many waveforms. We will discuss the estimation of the three constant parameters ($[K, P_0, \alpha]$) in Section 2.3 after showing an example of waveforms.

Example of waveforms from Envisat and AltiKa

One of the objectives of our analysis is to compare the precision of the arrival time estimates from Ka-band on-board of SARAL/AltiKa with the Ku-band altimeter. We use the Envisat altimeter for the comparison because AltiKa and Envisat share the same 35-day ground track. We also note that the waveform retracker developed here for AltiKa is based on the retracker developed by Garcia et al. (2014), so we can quantitatively compare the new AltiKa results with the Ku-band altimeter on-board of Envisat. The Envisat waveforms are provided at 18 Hz, and the AltiKa waveforms are provided at 40 Hz reflecting the ~ 2 times higher PRF of AltiKa with respect to Envisat.

The example of waveforms over the open ocean for both altimeters is shown in Figure 1. Both waveforms have 128 gates or samples that are equally spaced in time; 3.125 nanoseconds for Envisat and 2.381 nanoseconds for AltiKa. This corresponds to a range spacing of 0.47 m for Envisat and 0.31 m for AltiKa. Both sets of waveforms have a low noise power (P_o) prior to the sharp arrival of the main pulse, which begins nominally at gate 50. The AltiKa waveforms have a steeper trailing edge decay than Envisat because of the narrower antenna gain pattern. The noise in the waveforms appears higher at higher power level in accordance with (3). The Envisat waveform has power artifacts at very low (first 8) and high (last 18) gates, so these gates are excluded in the least-squares

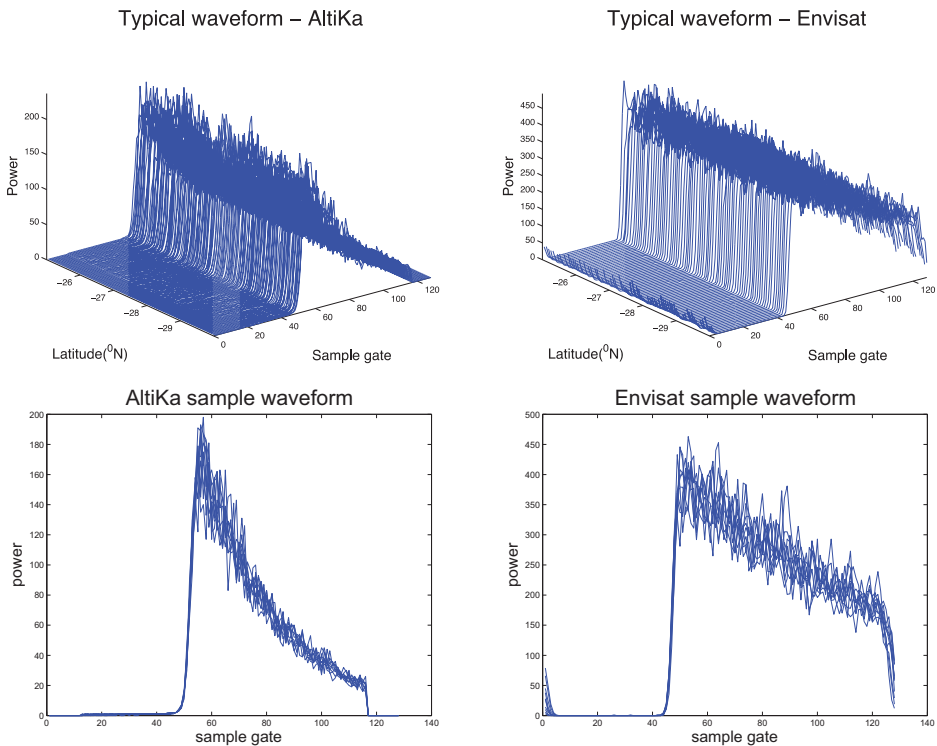


Figure 1. Waveform samples of the open ocean area for AltiKa (left) and Envisat (right).

analysis. Similarly, the first 12 and last 12 gates of the AltiKa waveform are all filled with zero value, so they are also not used.

Retracking waveforms from Envisat and AltiKa

As discussed previously, we begin the analysis with six unknown parameters ($[A, t_0, \sigma_h]$ and $[K, P_0, \alpha]$). The mathematical relationship between the model waveform and the unknown parameters is nonlinear, except the amplitude that has a linear relationship. We use an iterative weighted least-squares approach to solve for the arrival time parameter t_0 and the wave height parameter σ_h (Garcia et al. 2014). A threshold retracker is used to provide an initial estimate of t_0 , while the corresponding threshold value is defined with respect to the cumulative sum of waveform power. Actually, the two-pass retracking results through iterative fitting are largely insensitive to the threshold according to our experiments. Conversely, we determined the optimal threshold value by comparing with the two-pass retracking results, which led to the threshold values of 0.09 and 0.25, respectively, for AltiKa and Envisat. To estimate the three parameters ($[K, P_0, \alpha]$) that remain constant throughout the mission, we selected thousands of representative waveforms and searched this three-parameter space for the solution having the overall lowest misfit (2). For example, we swept through values of α at steps of $1.0e-4$. A best-fit α value of 0.0351 gate^{-1} was determined for AltiKa, while the best-fit α value for Envisat is 0.009 gate^{-1} . The same power offset value ($P_0 = 5500$) and number of statistically independent echoes ($K = 96$) were determined for both AltiKa and Envisat according to our experiments in optimizing the retracking. The power value for each gate is scaled by an arbitrary value of 3.3×10^6 to convert the original unsigned integers to floating point numbers. Based on analysis of misfit standard deviations and mean discrepancies with respect to threshold retracker results, we did not use the power in gates of 75–128 for AltiKa. This made the solution less sensitive to α variations and also improved the speed of the least-squares process. In accordance with the analysis by Garcia et al. (2014), we also found a significant improvement ($\sim 5\%$) in the 40-Hz range precision if the least-squares analysis was performed on three adjacent waveforms simultaneously, assigning the two outer waveforms $1/2$ the weight of the central waveform. Further enlargement of this three-waveform window did not reduce the range noise but increased processing time.

Examples of best fits to individual AltiKa and Envisat waveforms are provided in Figure 2. After examining thousands of waveforms over a range of sea states, we generally find that the visual fit to the AltiKa data is superior to the Envisat data, providing the first suggestion that the range precision of AltiKa is better than that of Envisat.

Once the standard three-parameter retracking algorithm was optimized for the three pre-determined constant parameters ($[K, P_0, \alpha]$), we retracked three complete cycles (35-day) using the two-pass method. The data are first retracked with the full three-parameter model. Then, the rise time parameter is low-pass filtered having a 0.5 gain at a full wavelength of 90 km. (Sandwell and Smith 2005; Garcia et al. 2014). The final step is to retrack the waveforms by fixing the rise time parameter to the smoothed value and only solving for the parameters of arrival time and amplitude.

Further processing is needed to eliminate bad records and make sure the input data are free from outliers before using the data to construct worldwide marine gravity models. As discussed in Raney and Phalippou (2011), the waveform of the Ka-band altimeter is highly

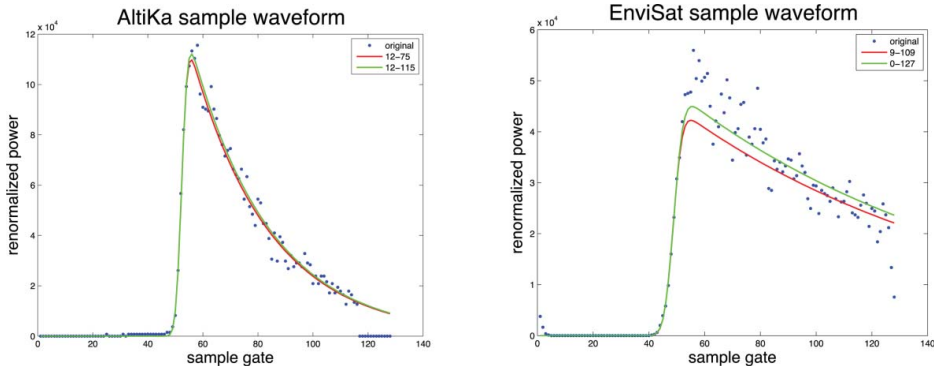


Figure 2. Least-squares fit of model waveform of AltiKa (left) and Envisat (right) for selected parameters. The green curves show fits for all the gates, while the red curves show fits when the range of gates is restricted.

sensitive to the liquid water content in the propagation path. Accordingly, we developed a waveform editing criteria based on estimated parameters ($[A, \sigma_h]$) as well as the fits to the waveforms. The editing threshold was established by constructing histograms of amplitude, chi-square misfit, and SWH versus standard deviation of the arrival time parameter. For AltiKa, valid waveforms should have a model amplitude within the range of 150000–180000, while the chi-squared misfit measurement should not exceed 1500. For Envisat, valid waveforms should have a model amplitude within the range 40000–80000, while the chi-squared misfit measurement should not exceed 800. We also removed waveforms having SWH outside of the range 0.3–10.0 m for both missions. An additional editing criterion for AltiKa uses the item of off-nadir angle (`off_nadir_angle_rain_40hz`), provided in the GDR, to detect records potentially affected by atmospheric liquid water (Tournadre et al. 2009). This parameter (`off_nadir_angle_rain_40hz`) varies along track with regular fluctuation between latitudes of 60°N and 60°S, while the variation at high latitudes is more irregular. An empirical choice of normal range from -0.018 to 0 is suggested for this parameter as another editing criterion except for polar ocean areas.

Evaluation and discussion

Noise level

To assess the noise level of AltiKa and Envisat data, we performed a statistical analysis on the retracked sea surface height values (altitude minus range). The corrections for path delay and geophysical environment are considered using items supplied by level 2 products. The noise was estimated as the standard deviation of the sea surface height with respect to the mean difference from the EGM2008 model computed over a 1-second interval. The EGM2008 model was used to account for areas of very steep geoid gradient where there could be a significant height variation (>20 mm) over the 7-km distance that the ground track moves in 1 second. For AltiKa, this involved the analysis of 40 estimates, while 18 estimates were used for Envisat, corresponding to along-track sample rates of AltiKa and Envisat, respectively. Figure 3 shows the AltiKa and Envisat noise levels for spatially coincident long passes across the Pacific Ocean (labeled 0002 and 00001 for AltiKa and Envisat separately). The noise in the arrival time of the leading edge of the waveform should increase

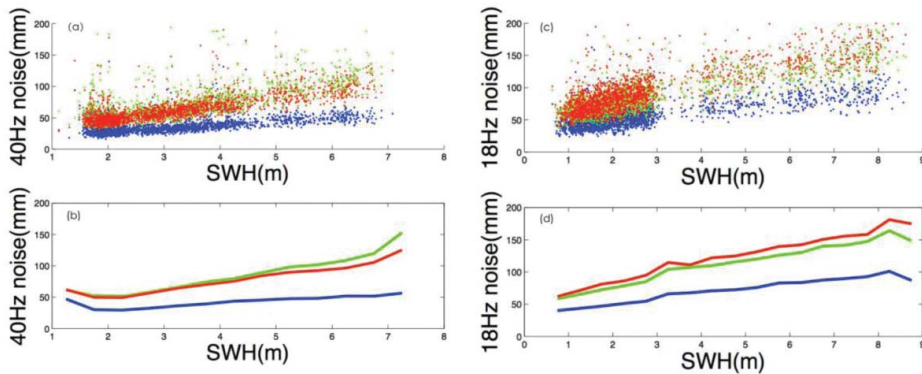


Figure 3. Standard deviation of retracked height with respect to EGM2008 for AltiKa (left) and Envisat (right) (red—geophysical data record; green—3-parameter retracking; blue—2-parameter retracking).

with increasing SWH, so we have plotted the data versus SWH (Figure 3). There are three independent estimates of this noise: the initial estimates in the GDR—range_{40Hz}—red dots); the estimates from our three-parameter retracking (green dots); and the noise from our two-parameter retracking (blue dots). The solid smoothed curves are median averages of these estimates in 0.5-m SWH bins. Generally, the noise levels of three-parameter and GDR retracked results are at a similar level. The noise level of the GDR is slightly lower than the three-parameter retracking for AltiKa, but it is a little higher for Envisat. The most important finding is that the noise level for two-parameter retracked data is significantly lower than that for three-parameter retracked data for both AltiKa and Envisat.

Under the typical conditions of 2-m SWH, mean values of standard deviation for GDR, three-parameter, and two-parameter results are, respectively, 49.8, 52.4, and 30.0 mm, for AltiKa, while they are 81.1, 72.4, and 47.0 mm for Envisat. When we restrict the analysis to records only between latitudes of 60°S and 60°N, AltiKa results are 49.7, 52.0, and 29.8 mm, while Envisat results are 81.3, 72.4, and 46.9 mm. This demonstrates that the two-parameter retracking of AltiKa decreases the noise level by a factor of 1.7 with respect to three-parameter retracking, while this ratio is about 1.5 for Envisat. Both results are very close to the expected noise reduction of 1.57 based on the Monte Carlo simulation (Sandwell and Smith 2005).

We expect that the altimeter noise will depend on environmental factors such as persistently high SWH, so we selected five large ($40^\circ \times 40^\circ$) geographical areas for a more complete noise analysis (Figure 4). This analysis was performed using three complete cycles of AltiKa. The results are shown in Figure 5 and summarized in Table 1. The noise levels in the five areas are not significantly different, suggesting that the editing criterion effectively removed outliers. Spikes sometimes occur when there are only a small number of observations involving the estimation in corresponding 0.5 m bin. In all the areas, noise for the two-parameter model is significantly lower than the three-parameter and GDR noise with an overall average reduction of 1.68 (Table 1). If we further assume that the 40 Hz range estimates from AltiKa are statistically independent, we infer a corresponding 20 Hz noise level that is the square root of 2 times lower than statistical results of 40 Hz range or 22 mm at 2 m SWH.

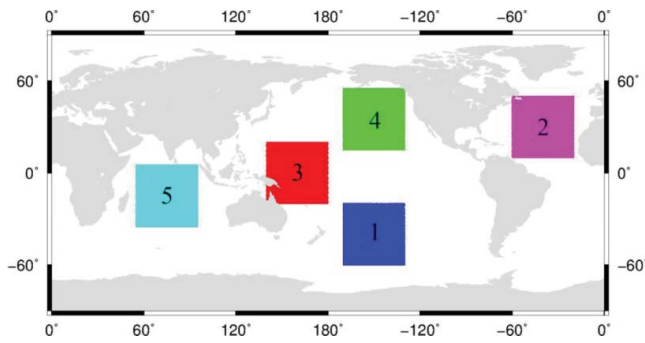


Figure 4. Five selected areas for AltiKa analysis of noise level.

Spectral analysis

Spectral analysis is an effective way of analyzing the signal and noise in the altimeter observations. Based on the Welch method (Welch 1967), the power spectral density of along-track sea surface height for three- and two-parameter retracked AltiKa data is estimated using MATLAB and shown in Figure 6a. Both spectra show a rapid increase in power for wavelengths greater than 40 km. Between wavelengths of 90 and ~ 5 km, the three- and two-parameter spectra form a “hump.” At wavelengths less than about 5 km, both the three- and two-parameter show a white noise floor. To highlight the differences between the two spectra, we calculated the spectra of the difference between the two- and three-parameter data as shown in Figure 6b. The increase in the difference spectra for wavelengths shorter than 90 km simply reflects the wavelength over which the SWH was smoothed between the three- and two-parameter retracking. At longer wavelengths, both retrackers provide the same height measurement because the profiles contain the same SWH signal. The “hump” in the difference spectra between the wavelengths of 90 and 5 km is also seen in spectra of the two- and three-parameter retracked data from Envisat, Jason-1, and CryoSat-2 LRM (Garcia et al. 2014). This is the band of wavelengths where two-pass retracking provides the most benefit (Sandwell and Smith 2005).

Comparison with global vertical deflection model

Another way of evaluating the precision of retracked profiles is by comparing along-track sea surface slope with the corresponding slope from the vertical deflection model V23.1 based on altimeter data of Geosat, ERS-1/2, Envisat, T/P, Jason-1, and CryoSat-2 (Sandwell et al. 2014). The RMS of slope differences with respect to the model provides the spatial distribution of the error. However, it is not an accurate estimate of the magnitude of the error in the AltiKa data because some of the differences will be due to mesoscale variability as well as errors in the gravity model. This procedure was accomplished by subtracting slopes of V23.1 vertical deflection grids from retracked altimeter slope profiles and applying a low-pass filter with a 0.5 gain at 18-km wavelength. A geoid slope correction was applied to the altimeter slope profile to account for the small but significant non-nadir reflection points in areas of steep geoid gradient (Sandwell and Smith 2013). After filtering, the RMS differences are averaged into 6-km cells. The results are shown in Figure 7 for both the three-parameter retracked data and the two-parameter retracked data. The median absolute deviation of the slope from the three-parameter data is 1.8 microradian. The largest deviations (>6

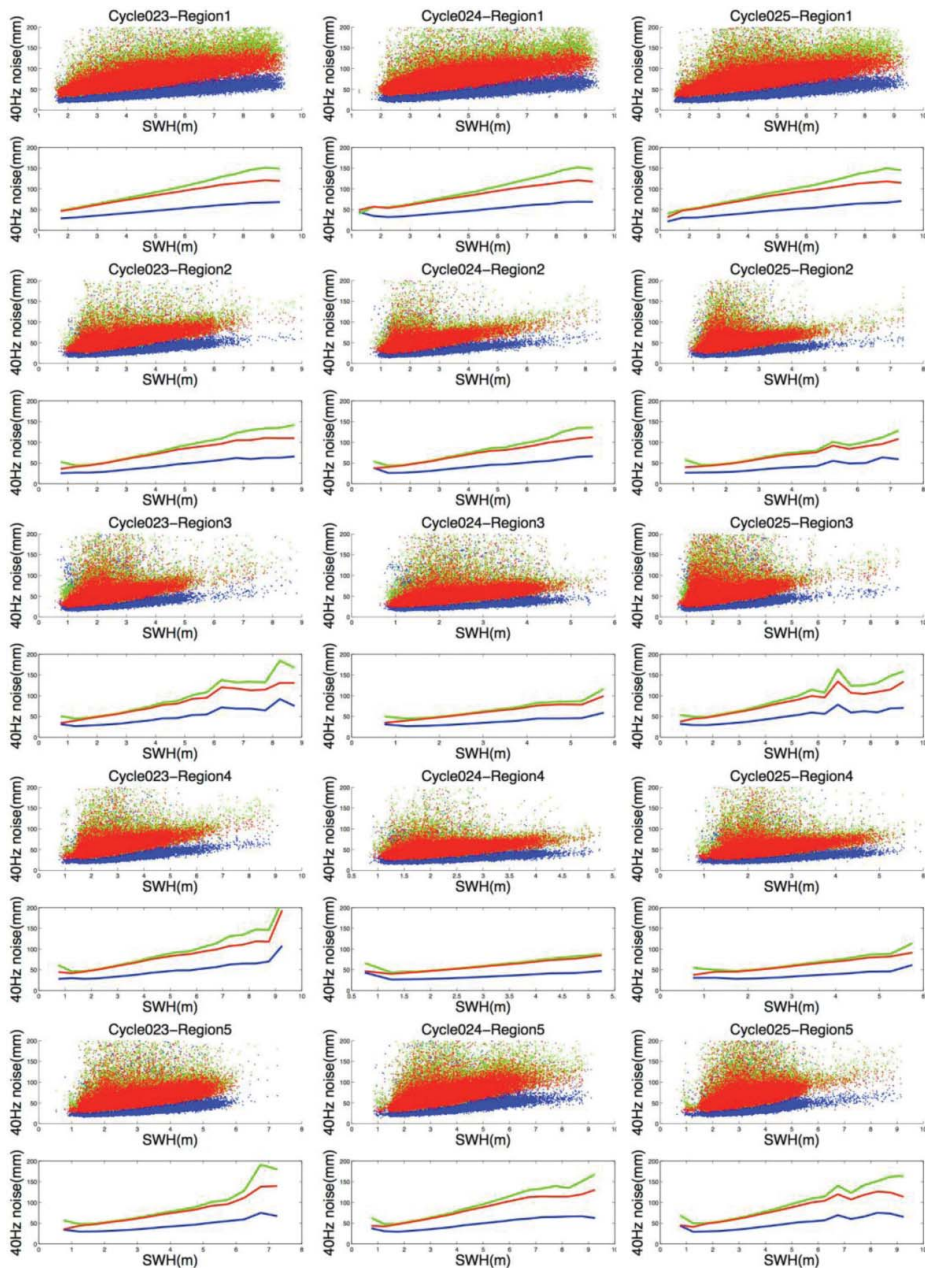


Figure 5. Standard deviation of retracked height estimates with respect to EGM2008 for AltiKa (red—geophysical data record; green—3-parameter retracking; blue—2-parameter retracking).

microradian) occur in the Arctic and Antarctic areas where the waveforms are contaminated by sea ice. There are other large deviations (>3 microradian) associated with the western boundary currents (e.g., Kuroshio, Gulf Stream, East Australian, Falkland) as well as the Antarctic Circumpolar Current (ACC). Large deviations (~ 3 microradian) also occur in areas of high sea state such as the North Atlantic and the Southern Ocean between 30°S and 60°S .

Table 1. 40-Hz altimeter noise of AltiKa within 5 selected areas (unit: mm).

Cycle	Region	2m SWH				6m SWH			
		GDR	3-para	2-para	3-para/2-para	GDR	3-para	2-para	3-para/2-para
23	1	46.496	48.268	28.960	1.67	76.179	81.014	42.929	1.89
	2	44.533	46.031	27.013	1.70	91.628	102.775	53.598	1.92
	3	46.008	47.908	28.162	1.70	94.907	108.504	54.700	1.98
	4	45.800	47.433	28.317	1.68	87.942	94.950	48.893	1.94
	5	47.945	49.963	30.254	1.65	95.930	106.248	55.129	1.93
24	1	57.041	56.113	34.782	1.61	92.480	102.253	52.150	1.96
	2	44.003	45.372	26.734	1.70	86.275	95.983	49.490	1.94
	3	45.326	47.149	27.604	1.71	99.160	116.175	58.936	1.97
	4	44.581	46.135	27.427	1.68	85.111	87.471	46.977	1.86
	5	47.525	49.149	29.342	1.68	99.746	109.966	54.773	2.01
25	1	47.651	49.974	30.302	1.65	93.413	103.111	52.363	1.97
	2	45.293	46.848	27.640	1.69	83.822	92.832	48.974	1.90
	3	47.198	49.231	29.098	1.69	99.368	114.300	59.473	1.92
	4	45.717	47.643	28.243	1.69	91.468	114.035	61.601	1.85
	5	48.955	50.596	30.066	1.68	99.975	109.370	54.146	2.02

The median absolute deviation of the two-parameter retracked data is smaller at 1.46 microradian. Large deviations (>3 microradian) also occur in areas of sea ice, western boundary currents, and the ACC. However, the deviations in the Southern Ocean and North Atlantic are much smaller (~ 2 microradian). This illustrates that the two-pass retracker performs best in areas of high sea state by stabilizing the estimates of SWH by along-track smoothing over ~ 45 -km distance. In low latitude areas, and enclosed bodies of water where swells are small, the median absolute deviation is commonly smaller than 1 microradian. For comparisons, we did a similar noise analysis for Envisat and Jason-1 and found a median absolute deviation of 1.85 and 1.74, respectively. So, even in the presence of ocean variability, the along-track slope from the AltiKa altimeter is at least 1.2 times better than the other Ku-band altimeters.

Discussion

The computer algorithm that was used to retrack the AltiKa data is identical to the algorithm used to retrack all the previous altimeter data published by Garcia et al. (2014). The main difference is that the AltiKa waveforms were provided at 40 Hz, and most of the other altimeter waveforms were provided at ~ 20 Hz (Geosat are available at 10 Hz). Table 2 shows a comparison of AltiKa noise with five other altimeters where we have scaled the AltiKa noise by the square root of 2 to account for the 2 times higher sampling rate. At 2-m SWH, the AltiKa noise level is 2.1 times smaller than the smallest value (CryoSat-2 LRM) for Ku-band altimeters (Garcia et al. 2014). Similarly, at 6-m SWH, the AltiKa noise level is 1.7 times better than that of Jason-1. One can question the assumption that the 40-Hz AltiKa waveforms are statistically independent. However, even without making this assumption, we find that AltiKa is far better than all the other altimeters at its full 40-Hz sampling rate. Another argument that the waveforms are statistically independent is that our estimate of 1-Hz noise (three-parameter at 2 m SWH) for AltiKa of 7.7 mm per root-Hz matches the estimate of 8 mm per root-Hz published by Smith (2015). Similarly, for Envisat, our value of 18.6 mm per root-Hz matches the value of 19 mm per root-Hz found in the study by Smith (2015). Hence, for the three-parameter retracking, we agree with Smith (2015) that the AltiKa noise

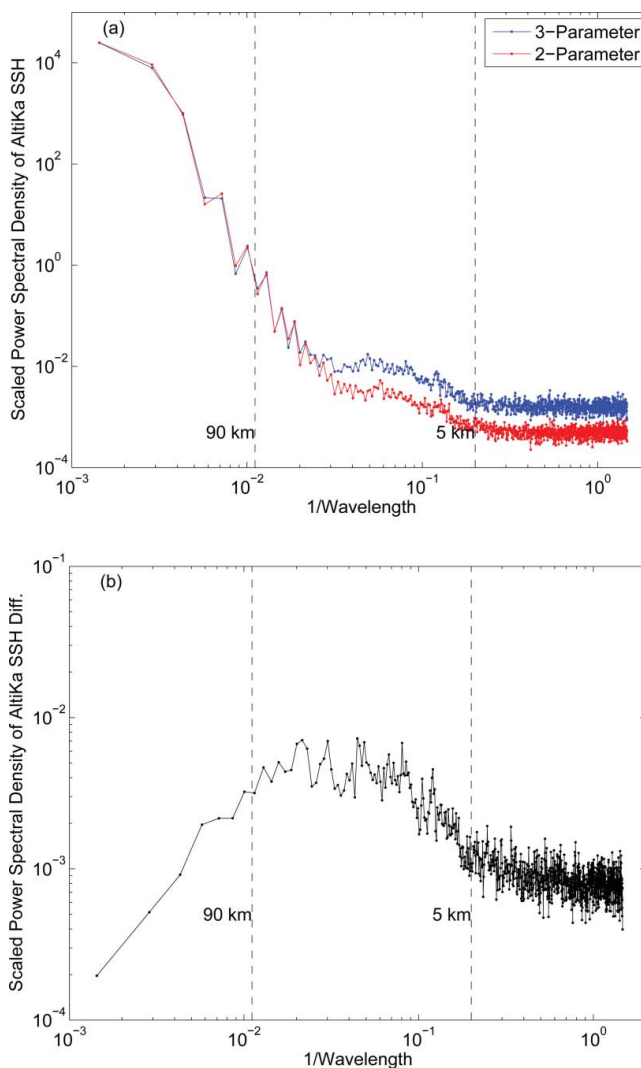


Figure 6. (a) Power spectral density of along track retracked height from 3-parameter (blue) and 2-parameter (red) model for AltiKa data. (b) Power spectral density of along track retracked height difference between 3-parameter and 2-parameter model for AltiKa data. Wavelength range of spectral hump 5–90 km marked by vertical dashed lines.

is less than half of the Envisat noise. The new result from our analysis is that the double retracking further reduces the noise by a factor of 1.67 to an extremely low value of just 4.6 mm per root-Hz.

The error in the gravity field along an altimeter track depends on the error in the sea surface slope measurement. One milligal of gravity error corresponds to ~ 1 microradian of sea surface slope error. The recent altimeter-derived gravity models have a spatial resolution ($1/2$ wavelength) of ~ 6 km (Andersen and Knudsen 2010). Over a 1-second interval, the footprint of a radar altimeter moves about 6 km, so the along-track ocean surface noise from AltiKa corresponds to 0.8 microradian or ~ 0.8 milligal. The recent altimeter-derived gravity models have accuracies of ~ 2 milligal in the open ocean and 1.6 milligal in the Gulf of

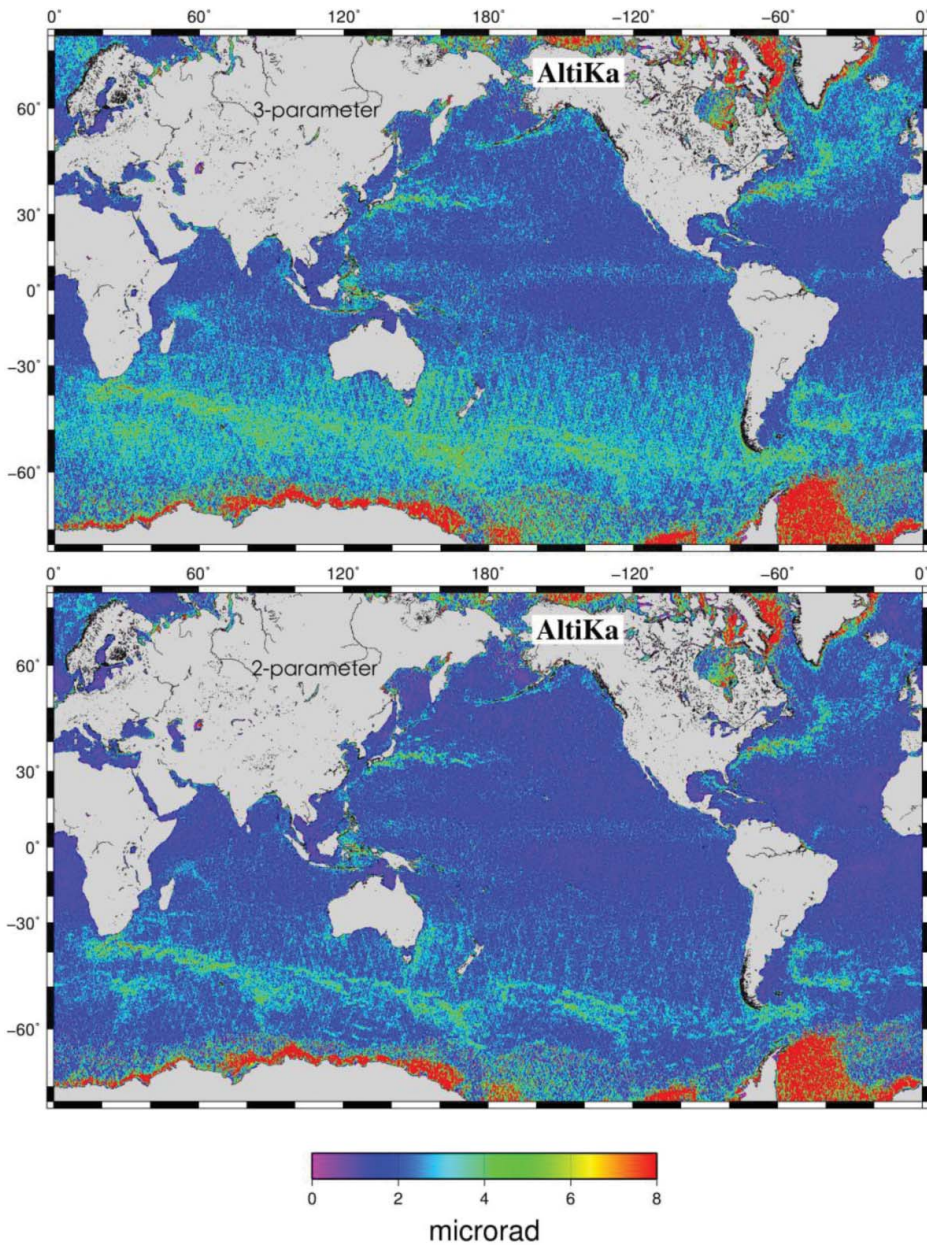


Figure 7. Median absolute differences between slopes from the gravity model V23.1 and those from the 3-parameter (top) and 2-parameter (bottom) retracked AltiKa profiles.

Mexico where the SWH is generally lower (Sandwell et al. 2014). The two-dimensional accuracy of the gravity field also depends on the spacing between the tracks, so the spacing must be ~ 6 km or smaller to match the 6-km along-track resolution. As a result, SARAL has been placed in non-repeating orbit (geodetic phase) since July 2016. In this orbit, a ~ 6 -km average track spacing will be obtained after 1.3 years, providing approximately one complete coverage for gravity recovery. Of course, a longer mapping mission would result in an

Table 2. 20-Hz altimeter noise for most of the altimeters (unit: mm).

Altimeter	3-para at 2 m	2-para at 2 m	3-para/2-para	2-para at 6 m
Geosat	88.0	57.0	1.54	105.4
ERS-1	93.6	61.8	1.51	111.8
Envisat	78.9	51.8	1.52	88.6
Jason-1	75.9	46.4	1.64	64.2
CryoSat-2 LRM	64.7	42.7	1.52	71.7
CryoSat-2 SAR	49.5	49.7	.996	110.9
AltiKa	34.3 (48.5)	20.5 (28.9)	1.68	37.4 (52.9)

Standard deviation of altimeter waveforms with respect to the 1-Hz average. The non-AltiKa analysis was published in Garcia et al. (2014). The AltiKa results are the average of all the estimates provided in Table 1. The values in parentheses are the 40-Hz noise estimates, while the bold values have been scaled by the square root of 2 for comparison with the other altimeters.

additional improvement. By contrast, it would take a state-of-the-art Ku-band altimeter 4 times longer (~ 5 years) to achieve the same accuracy, while assuming all other factors are equal. Actually, the Ku-band measurements of Jason-1 geodetic mission did a better job with the east-west gradient due to its lower inclination than AltiKa.

It has been proposed that a SAR altimeter such as CryoSat-2 (CS2) could achieve the same level of range precision as has been achieved by AltiKa (Raney and Phalippou 2011). Unfortunately, CS2 operates in a closed-burst mode where 64 pulses are emitted, and then, pulsing stops until the echoes of these 64 have been recorded. This causes the radar to operate only about 1/3 of the time, and it results in suboptimal range precision (Raney and Phalippou 2011; Raney 2012). In addition, because of the more complex shape of the SAR waveform, the arrival time and SWH are not strongly correlated during the least-squares waveform fitting. Therefore, as shown in Garcia et al. (2014), the SAR-mode data do not benefit from two-pass retracking. If CS2 or a future altimeter was operated in an open-burst mode, it could achieve range precision similar to the AltiKa precision, so these two new technologies will be competitive in the case of gravity field recovery.

Conclusions

The innovative design of the AltiKa altimeter provides a factor of 2 improvement in range precision with respect to all previous altimeter missions. This factor of 2 improvement was demonstrated in a previous study using the GDR measurements provided in the level-2 data products (Smith 2015). These standard GDR data are based on MLE3-4 retracking, which is suboptimal for gravity field investigations. We show that the two-pass retracking method provides an additional factor of 1.7 improvement in range precision. The overall conclusion is that the range precision of AltiKa is more than 2 times better than that of previous altimeters, and with dense ocean coverage, this could translate into a global marine gravity model that is significantly better than models available today.

For the first 3 years of its mission, the SARAL satellite was in the same 35-day repeat orbit as Envisat. However, in the spring of 2015, its orbit began to drift by up to 10 km from the 35-day track. This has resulted in a few cycles of new ocean coverage with Ka-band altimetry. As of July 2016, the orbit is drifting, so it no longer maintains the 35-day track. If the orbit drifts for 1.3 years or longer, we could have a factor of 1.5 improvement in the accuracy of the global marine gravity field. Moreover, a dedicated Ka-band mission could result in

additional gains in accuracy although these repeated measurements would only provide incremental improvements as the square root of the number of times the 1.3-year ground track was repeated. The next big step in gravity field improvement may come with the higher range precision provided by SWOT, which scheduled for launch in 2020 (Fu and Ubelmann 2013).

Acknowledgements

The authors thank the two reviewers for their extensive comments that greatly improved the clarity of this paper.

Funding

The SARAL/AltiKa data were provided by CNES, and Envisat data were provided by the European Space Agency. Zhang was supported by 973 Project of China (No.2013CB73301, No.2013CB73302), National Natural Science Foundation of China (No.41210006, No.41304003), and the project of Key Laboratory of Geospace Environment and Geodesy, Ministry of Education, China (No.20150209). Sandwell was supported by the National Geospatial-Intelligence Agency (HM0177-13-1-0008) and NASA SWOT program (NNX16AH64G).

References

- Abramowitz, M., and I. A. Stegun. 1964. *Handbook of Mathematical Functions with Formulas, Graphs, and Mathematical Tables*. Washington, DC: U.S. Government Printing Office, p.1045.
- Amarouche, L., P., Thibaut, O. Z. Zanife, J.-P. Dumont, P. Vincent, and N. Steunou. 2004. Improving the Jason-1 ground retracking to better account for attitude effects. *Marine Geodesy* 27:171–197.
- Andersen, O. B., P. Knudsen, and P. Berry. 2010. The DNSCO8GRA global marine gravity field from double retracked satellite altimetry. *Journal of Geodesy* 84(3):191–199. doi: 10.1007/s00190-009-0355-9
- Andersen, O. B., and P. Knudsen. 1998. Global marine gravity field from the ERS-1 and Geosat geodetic mission altimetry. *Journal of Geophysical Research* 103(C4):8129–8137.
- Bendat, J. S., and A. G. Piersol. 1986. *Random Data—Analysis and Measurement Procedures*, 2nd ed. New York: John Wiley and Sons, p. 566.
- Brown, G. 1977. The average impulse response of a rough surface and its applications. *IEEE Transactions on Antennas and Propagation* 25(1):7–74.
- Chelton, D. B., J. W. Edward, and J. L. MacArthur. 1989. Pulse compression and sea level tracking in satellite altimetry. *Journal of Atmospheric and Oceanic Technology* 6:407–438.
- Chelton, D. B., J. C. Ries, B. J. Haines, L.-L. Fu, and P. S. Callahan. 2001. Satellite altimetry. In *Satellite Altimetry and Earth Sciences*. Fu, L.-L., and A. Cazenave (eds.), San Diego, CA: Academic Press, 1–131.
- Davis, C. H. 1995. Growth of the Greenland ice sheet: A performance assessment of altimeter retracking algorithms. *IEEE Transactions on Geoscience and Remote Sensing* 33(5):1108–1116.
- Fu, L. L., and C. Ubelmann. 2013. On the transition from profile altimeter to swath altimeter for observing global ocean surface topography. *Journal of Atmospheric and Oceanic Technology* 31:560–568. doi: 10.1175/JTECH-D-13-00109.1
- Garcia, E. S., D. T. Sandwell, and W. H. F. Smith. 2014. Retracking CryoSat-2, Envisat, and Jason-1 radar altimetry waveforms for improved gravity field recovery. *Geophysical Journal International* 196(3):1402–1422.
- Haxby W. F., G. D. Karner, J. L. LaBrecque, and J. K. Weissel. 1983. Digital images of combined oceanic and continental data sets and their use in tectonic studies. *Eos, Transactions American Geophysical Union* 64(52):995–1004.
- Hayne, G. 1980. Radar altimeter mean return waveforms from near-normal-incidence ocean surface scattering. *IEEE Transactions on Antennas and Propagation* 28(5):687–692.

- Hwang, C., J. Guo, X. Deng, H. Y. Hsu, and Y. Liu. 2006. Coastal gravity anomalies from retracked Geosat GM altimetry: improvement, limitation and the role of airborne gravity data. *Journal of Geodesy* 80(4):204–216.
- Hwang, C., E. C. Kao, and B. Parsons. 1998. Global derivation of marine gravity anomalies from Seasat, Geosat, ERS-1 and Topex/Poseidon altimeter data. *Geophysical Journal International* 134(2):449–459.
- Idris, N. H., and X. Deng. 2012. The retracking technique on multi-peak and quasi-specular waveforms for Jason-1 and Jason-2 missions near the coast. *Marine Geodesy* 35(sup1):217–237.
- Laxon, S., and D. McAdoo. 1994. Arctic ocean gravity field derived from ERS-1 satellite altimetry. *Science* 265(5172):621–624.
- Marks, K. M., and R. V. Sailor. 1986. Comparison of GEOS-3 and SEASAT Altimeter Resolution Capabilities. *Geophysical Research Letters* 13(7):697–700.
- Martin, T. V., H. J. Zwally, A. C. Brenner, and R. A. Bindshadler. 1983. Analysis and retracking of continental ice sheet radar altimeter waveforms. *Journal of Geophysical Research* 88(C3):1608–1616.
- Maus, S., C. M. Green, and J. D. Fairhead. 1998. Improved ocean-geoid resolution from retracked ERS-1 satellite altimeter waveforms. *Geophysical Journal International* 134(N1):243–253.
- Passaro, M., P. Cipollini, S. Vignudelli, G. D. Quartly, and H. M. Snaith. 2014. ALES: A multi-mission adaptive subwaveform retracker for coastal and open ocean altimetry. *Remote Sensing of Environment* 145:173–189.
- Prandi, P., S. Philipps, V. Pignot, and N. Picot. 2015. SARAL/AltiKa global statistical assessment and cross-calibration with Jason-2. *Marine Geodesy* 38:297–312. doi: 10.1080/01490419.2014.995840
- Raney, R. K., and L. Phalippou. 2011. The future of coastal altimetry. In *Coastal Altimetry*. Vignudelli, S., A. G. Kostianoy, P. Cipollini, and J. Benveniste (eds.), 535–560. Berlin/Heidelberg: Springer-Verlag. doi: 10.1007/978-3-642-12796-0_20
- Raney, R. K. 2012. Cryosat SAR mode looks revisited. *IEEE Transactions on Geoscience and Remote Sensing* 9(3):393–397. doi: 10.1109/LGRS.2011.2170052
- Rapp R. H. 1979. Geos 3 data processing for the recovery of geoid undulations and gravity anomalies. *Journal of Geophysical Research* 84(B8):3784–3792.
- Rodríguez, E. 1988. Altimetry for non-Gaussian oceans: Height biases and estimation of parameters. *Journal of Geophysical Research: Oceans* 93(C11):14107–14120.
- Sandwell D. T., and W. H. F. Smith. 1997. Marine gravity anomaly from Geosat and ERS 1 satellite altimetry. *Journal of Geophysical Research* 102(B5):10039–10054.
- Sandwell, D. T., and W. H. F. Smith. 2005. Retracking ERS-1 altimeter waveforms for optimal gravity field recovery. *Geophysical Journal International* 163(1):79–89.
- Sandwell, D. T., and W. H. F. Smith. 2013. Slope correction for ocean radar altimetry. *Journal of Geodesy* 88(8):765–771. doi: 10.1007/s00190-014-0720-1
- Sandwell, D. T., R. D. Müller, W. H. F. Smith, E. Garcia, and R. Francis. 2014. New global marine gravity model from CryoSat-2 and Jason-1 reveals buried tectonic structure. *Science* 346(6205):65–67.
- Sarrailh, M., G. Balmino, and D. Doublet. 1997. The arctic and Antarctic oceans gravity field from ERS1 altimetric data. *International Association of Geodesy Symposia* 117:437–444.
- Smith, W. H. F. 2015. Resolution of seamount geoid anomalies achieved by the SARAL/AltiKa and Envisat RA2 satellite radar altimeters. *Marine Geodesy* 38:644–671.
- Steunou, N., J. D. Desjonqueres, N. Picot, P. Sengenés, J. Noubel, and J. C. Poisson. 2015. AltiKa altimeter: instrument description and in flight performance. *Marine Geodesy* 38:22–42. doi: 10.1080/01490419.2014.988835
- Tournadre, J., J. Lambin, and N. Steunou. 2009. Cloud and rain effects on ALTIKA/SARAL Ka band radar altimeter, Part 1: Modeling and mean annual data availability. *IEEE Transactions on Geoscience and Remote Sensing* 47(6):1806–1817.
- Verron, J., P. Sengenés, J. Lambin, J. Noubel, N. Steunou, A. Guillot, N. Picot, S. Coutin-Faye, R. Sharma, R. M. Gairola, and D. R. Murthy. 2015. The SARAL/AltiKa altimetry satellite mission. *Marine Geodesy* 38:2–21.
- Welch, P. D. 1967. The use of fast Fourier transforms for the estimation of power spectra: a method based on time averaging over short, modified periodograms. *IEEE Transactions on Audio Electroacoustics* 15:70–73.

- Wingham, D. J., C. G. Rapley, and H. Griffiths. 1986. New techniques in satellite altimeter tracking systems. *ESA Proceedings of the 1986 International Geoscience and Remote Sensing Symposium on Remote Sensing: Today's Solutions for Tomorrow's Information Needs*, Zürich, Switzerland, 1339–1344.
- Vincent, P., N. Steunou, E. Caubet, L. Phalippou, L. Rey, E. Thouvenot, and J. Verron. 2006. AltiKa: a Ka-band altimetry payload and system for operational altimetry during the GMES period. *Sensors* 6:208–234.